Astronomical Image Segmentation in Computer Vision for Automated Object Detection and Classification

Sergii V. Khlamov [1,*], Vadym E. Savanevych [2], Vladimir P. Vlasenko [3], Oleksandr B. Briukhovetskyi [4], and Tetiana O. Trunova [1]

[1] Department of Media Systems and Technologies, Faculty of Computer Science, Kharkiv National University of Radio Electronics, Kharkiv, Ukraine
[2] Department of Systems Engineering, Faculty of Computer Science, Kharkiv National University of Radio Electronics, Kharkiv, Ukraine
[3] Space Research and Communication Center, National Space Facilities Control and Test Center, Kyiv, Ukraine
[4] Western Center of Radio Engineering Surveillance, National Space Facilities Control and Test Center, Mukachevo, Ukraine
Email: sergii.khlamov@gmail.com (S.V.K.); vadym.savanevych1@nure.ua (V.E.S.); vlasenko.vp@gmail.com (V.P.V.); oleksandr.briukhovetskyi@gmail.com (O.B.B.); tetiana.trunova@nure.ua (T.O.T.)
*Corresponding author

***Abstract*—Automated analysis of astronomical images has become increasingly important due to the growing volume of data generated by modern sky surveys and observatories. This paper presents an image segmentation approach designed to improve the automated detection and classification of objects in astronomical frames. The approach combines classical image processing and modern computer vision techniques to isolate and characterize objects of interest, even in the presence of noise, telescope aberrations, low contrast, or overlapping sources commonly found in wide-field images. The segmentation pipeline employs adaptive thresholding, background subtraction, and morphological filtering to enhance the visibility of both point-like and extended sources. The classification process enables the differentiation between various imaging artifacts and celestial objects, including stars, galaxies, Small Solar System Objects (asteroids, comets), and even artificial satellites. The paper describes the modern features for astronomical image processing implemented in the Lemur software within the scope of the Collection Light Technology (CoLiTec) project (https://colitec.space). The Lemur software is designed to perform a sequence of the following main steps: data mining, classification, background alignment, brightness equalization, image segmentation, typical shape analysis, pattern recognition, object detection/identification, astrometric/photometric reduction, and trajectory detection. The Lemur software has facilitated over 1700 discoveries of asteroids, including 5 Near-Earth objects, 21 Trojan asteroids of Jupiter, and 1 Centaur. In total, it has been used in about 800,000 observations, during which five comets were discovered.**

***Keywords*—image processing, filtering, segmentation, classification, pattern recognition, data mining, knowledge discovery, big data, astronomy**

I. Introduction

The automated analysis of astronomical images [1] has become essential in the era of data-intensive astronomy [2].

With the growing scale of sky surveys and observational campaigns, modern observatories routinely generate terabytes of imaging data, capturing a wide range of celestial phenomena—from stellar fields and galaxies to transient and moving objects [3] like Solar System Objects (SSOs) such as asteroids [4], comets, Near-Earth objects (NEOs) [5].

To process the vast amount of astronomical data [6], the field has increasingly relied on digital image processing [7] and computer vision methods [8]. Among these, image segmentation plays a critical role by isolating meaningful regions of interest that correspond to physical objects in the sky.

Conventional segmentation methods, such as thresholding or region-growing, have been widely applied to astronomical data with varying degrees of success.

However, these approaches often struggle under conditions typical of wide-field Charge-Coupled Device (CCD) imagery (Fig. 1) [9]: low signal-to-noise ratios, overlapping sources, irregular backgrounds, and the presence of both faint and extended structures.

Moreover, traditional algorithms [10] are often tailored to specific types of objects or observational conditions, limiting their generalizability across diverse datasets.

These limitations reveal a critical gap: the need for robust and adaptable segmentation techniques that can support automated object detection [11] and classification under real-world observational constraints.

Manuscript received August 7, 2025; revised August 28, 2025; accepted November 11, 2025; published March 26, 2026.

Fig. 1. The standard telescope structure.

Addressing this gap is crucial not only for improving the accuracy of astronomical object catalogs but also for enabling the timely identification of rare or transient events, such as NEOs, variable stars [12], or artificial satellites [13].

The objective of this paper is to develop a framework for segmentation and classification within the computer vision paradigm, enhancing the automated analysis of astronomical CCD images. The approach integrates classical image processing [14] with domain-specific heuristics to address the unique challenges of astronomical data mining [15].

It has been implemented in the Lemur software [16], developed under the Collection Light Technology (CoLiTec) project (https://colitec.space) [17], which has already contributed to the discovery of numerous asteroids and comets. By improving the segmentation foundation, the system supports more reliable classification and facilitates downstream tasks such as astrometry [18], photometry [19], and scientific reporting.

The remainder of this paper is organized as follows: Section II reviews related work; Section III describes the segmentation and classification methodology; Section IV outlines the experimental setup, presents the results of research, discusses applications and provides a broader discussion; and Section V concludes the study.

II. Literature Review

Astronomical image segmentation has long been a foundational task in observational astronomy, supporting critical workflows such as object detection, classification, and tracking. Early segmentation tools and pipelines relied on thresholding, region-growing, and morphological filters to isolate sources from the background. Among these, SExtractor [20] remains a standard, offering robust photometric analysis and source extraction in a wide range of sky surveys. Despite its success, SExtractor's performance often deteriorates in the presence of overlapping objects, non-uniform backgrounds, or low signal-to-noise ratios typical of wide-field CCD observations.

To support amateur and professional astronomers in CCD image analysis, several user-oriented tools have emerged. One such tool, MaxIm DL (https://diffractionlimited.com/maxim-dl) [21], provides an integrated environment for astronomical image calibration, alignment, and photometry. While it includes basic object detection and centroiding features, its segmentation capabilities are relatively limited and primarily optimized for manual or semi-automated workflows. Object identification in MaxIm DL relies on brightness thresholds and predefined parameters, which can lead to inaccuracies when processing faint, extended, or overlapping sources. It is mainly used for routine observations and is not optimized for high-throughput automated pipelines.

Another widely used tool, Astrometrica (http://astrometrica.at) [22], is designed for astrometric reduction and the manual detection of moving objects, such as asteroids or artificial satellites. Astrometrica supports the blinking of image sequences, allowing users to mark and measure the positions of suspected moving bodies. However, the segmentation and detection process are predominantly manual, with minimal automation. As such, while Astrometrica is valuable for discovery verification and astrometry, it lacks the adaptive segmentation strategies necessary for high-volume detection and classification.

Other traditional algorithms, including matched filters [23] and watershed-based segmentation, have demonstrated success in specific contexts but generally require careful parameter tuning and suffer from limited generalizability. For example, these methods often assume point-like source morphology, which makes them less effective in processing wide-field images containing galaxies, nebulosity, and diffuse background structures.

Recent developments in computer vision have introduced more sophisticated techniques for segmentation [24], such as edge detection, multi-scale morphological filtering, and structure-based region growing. These methods have improved robustness under challenging conditions, including crowded fields and variable backgrounds. However, many implementations still rely on static rules or require extensive manual intervention, which hinders their application in large-scale surveys.

Furthermore, although deep learning [25, 26] has shown promise in astronomical image analysis, its reliance on large, labeled training datasets and significant computational resources limits its use in routine observational pipelines, especially for the discovery of rare or unpredictable phenomena.

These limitations highlight the need for hybrid segmentation systems that can combine the efficiency of classical techniques with the adaptability of computer vision and image recognition [27]. The proposed system in this study addresses these gaps through a modular pipeline capable of robust segmentation and classification across a variety of object types and imaging conditions, while maintaining computational efficiency suitable for real-time or batch-mode operation.

III. Materials and Methods

A. Image Artifacts and Frame Corruption in Astronomical Imaging

Astronomical CCD frames are subject to various forms of corruption that significantly complicate automated image analysis (Fig. 2). These distortions can arise from both instrumental limitations and environmental conditions, introducing noise, inconsistencies, or false structures that interfere with object detection, segmentation and classification.

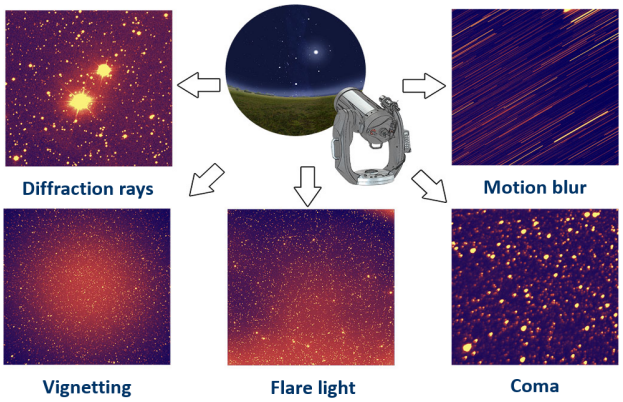

Fig. 2. Image artifacts and frame corruption in astronomical imaging.

One of the most common types of corruption is background non-uniformity, caused by atmospheric gradients, vignetting, or scattered light.

Such uneven illumination can mislead global thresholding algorithms and suppress the visibility of faint sources. Bias instability and dark current fluctuations also contribute to pixel-level noise patterns, particularly in long-exposure images or during temperature variation in the CCD sensor.

Cosmic rays represent another frequent artifact, manifesting as sharp, localized spikes in brightness that mimic or obscure real astronomical sources. These high-energy particles can impact individual pixels or small regions, often requiring statistical or morphological filtering for suppression.

Saturation and blooming effects occur when bright stars exceed the sensor's dynamic range, producing vertical or horizontal streaks that may overlap with nearby, fainter sources. Similarly, hot and dead pixels, resulting from sensor defects or aging, introduce fixed noise patterns that distort the integrity of the image.

Star trails or motion blur, typically caused by tracking errors, poor mount alignment, or long exposures without proper compensation, lead to elongated or smeared source shapes. This impairs both segmentation accuracy and subsequent photometric measurements.

In multi-frame observations, frame-to-frame misalignment, variable seeing conditions, and differential sky backgrounds can introduce inconsistencies that affect co-registration and source matching. Artificial objects such as satellites or space debris may also appear as streaks or transient artifacts that require separate handling.

These challenges necessitate a pre-processing and segmentation approach that is adaptable, noise-tolerant, and capable of preserving faint or partially corrupted sources while rejecting spurious detections. The following subsections describe the methods developed and implemented in the Lemur software [28] to address these issues within the context of automated astronomical image analysis.

B. Segmentation and Contouring for Object Image Pattern Detection

Following the suppression of background inconsistencies and artifacts during pre-processing, the next critical step involves segmenting astronomical frames to isolate object images and derive their morphological patterns. The primary goal of segmentation is to identify connected pixel regions corresponding to real celestial sources, while minimizing false detections caused by noise or residual artifacts.

The segmentation process begins with adaptive thresholding, where each pixel is compared against a locally estimated background intensity level. This method accommodates gradual background variations across the field of view, improving the detectability of both faint and bright sources. A two-pass strategy is employed: a conservative threshold is used to ensure the detection of high-confidence objects, followed by a relaxed threshold to capture fainter structures, which are then filtered through morphological criteria.

Once thresholding identifies candidate regions, morphological filtering is applied to refine them. Operations such as opening and closing help eliminate noise spikes and bridge the gaps between fragmented parts of extended objects. Erosion and dilation are also used to consolidate object boundaries and separate partially overlapping sources.

Detected objects are then passed to a contouring algorithm, which traces the pixel boundary of each segmented region. The resulting contours are stored as closed vector paths and serve as the basis for computing geometric and photometric descriptors. These contours capture the object image's pattern—a two-dimensional projection of its brightness structure—which is essential for distinguishing between stars, galaxies, comets, asteroids, and spurious detections (Fig. 3).

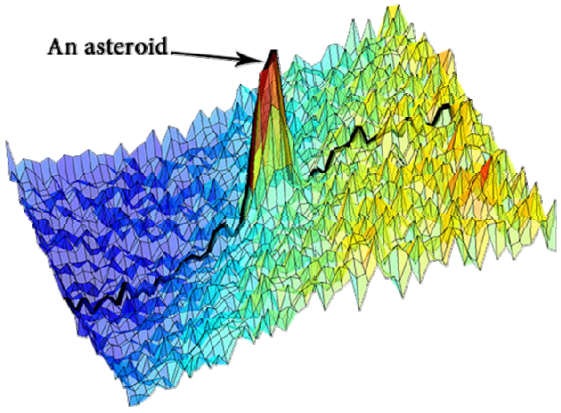

Fig. 3. Brightness measuring in the object image.

Each segmented object is characterized by a set of properties derived from its contour:

- Shape descriptors: area, elongation, eccentricity, roundness;
- Centroid coordinates and bounding box;
- Pixel intensity distribution and peak flux;
- Radial symmetry and edge sharpness.

In the context of moving object detection (e.g., asteroids or artificial satellites [29]), the extracted patterns can be compared across a sequence of frames to track positional shifts and verify the consistency of linear motion. Static background objects, in contrast, preserve their relative positions and serve as a reference for astrometric calibration [30].

This segmentation and contour extraction pipeline ensure that object patterns are not only detected accurately but also encoded in a form suitable for downstream classification and trajectory analysis. The robustness of the contour-based representation allows the system to adapt to a wide range of object morphologies, including diffuse galaxies, stellar PSFs, elongated streaks, and irregularly shaped transients.

C. Object Image Pattern Types in Astronomical Segmentation

Segmented regions in astronomical CCD frames exhibit diverse morphologies depending on the type of object, its brightness, apparent motion, and observational conditions. To enable accurate classification and identification, the extracted object images are categorized into several pattern types based on the geometry of their contours, intensity profiles, and structural coherence. These patterns reflect both the physical properties of the sources and instrumental effects, serving as the basis for filtering, tracking, and scientific interpretation.

The following four categories represent the most frequently encountered object image patterns in wide-field astronomical imaging: circular, elongated, with intersection and blurred (Fig. 4).

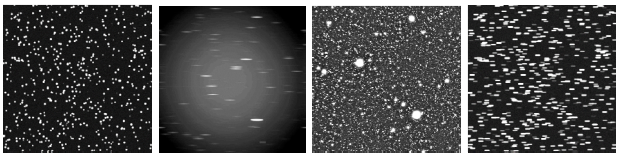

Fig. 4. Object image pattern types in astronomical segmentation.

1) Circular pattern

Circular or nearly circular contours are typically associated with point-like sources, such as stars or distant compact galaxies. These objects often produce well-centered, symmetric brightness distributions resembling the Point Spread Function (PSF) of the optical system. The key descriptors include:

- High roundness and low eccentricity;
- Bright central peak with radial symmetry;
- Small, well-defined contour area.

Circular patterns are also used as reference stars [31] for astrometric calibration due to their stable position and consistent morphology across frames.

2) Elongated pattern

Elongated shapes frequently indicate moving objects, such as asteroids, artificial satellites, or comets with visible motion during the exposure.

They may also arise from tracking errors, long exposure times (resulting in star trails), edge-on galaxies, or binary star systems. Elongated patterns are characterized by:

- High aspect ratio and elongation;
- Linear or elliptical contours;
- Gradient along the central axis of the shape.

These patterns are fundamental in multi-frame analysis, where their orientation and length help determine motion vectors and verify consistency with orbital models.

3) Intersecting pattern

In crowded fields or near the galactic plane, object images may overlap or intersect, forming compound structures that challenge segmentation accuracy.

Intersections can occur between: closely spaced stars, stars and galaxies or objects superimposed on background nebulosity or noise. Features of intersecting patterns include:

- Irregular, non-convex boundaries;
- Multiple intensity peaks within a single contour;
- Ambiguous centroid or shape parameters.

Special handling, such as multi-object deblending or hierarchical segmentation, is often required to separate intersecting sources and attribute correct photometric and positional data.

4) Blurred pattern

Blurring arises from a combination of instrumental and environmental effects, including: atmospheric turbulence (seeing), optical defocus or aberration, and motion-induced smearing (e.g., slow drift or jitter). Blurred patterns typically display:

- Low contrast with diffuse edges;
- Flattened or asymmetric intensity profiles;
- Difficulty in defining sharp boundaries or centroid location.

Blurred objects may be genuine sources (e.g., faint galaxies or comets with halos) or degraded images of point sources.

Their identification requires careful analysis of background-subtracted profiles and contour smoothness metrics.

D. Object Typical Image Shape

The mentioned above object image pattern types serve as input for downstream filters that distinguish between celestial sources and artifacts, and prioritize objects for further astrometric and scientific processing [32].

Suppose the typical shape of an object image in a CCD frame cannot be classified under the above common astronomical segmentation pattern types. In that case, it should instead be determined using the object's eccentricity, image length and inclination angle as key descriptors.

Eccentricity is a measure of how elongated an object's image is compared to a perfect circle. It ranges from 0 (a circle) to 1 (a very stretched ellipse).

Image length is the major-axis size of the object's image, representing its longest visible dimension in pixels.

Inclination angle is the orientation of the object's major axis relative to a reference direction, showing how the image is rotated in the frame.

For every image in the list of bright object images, the eccentricity ε_m of the object's image is computed individually:

$$\varepsilon_m = \frac{m_{20} + m_{02} - \sqrt{m_{20} - m_{02} + 4m_{11}^2}}{m_{20} + m_{02} + \sqrt{m_{20} - m_{02} + 4m_{11}^2}} \tag{1}$$

where m is the second-order moment:

$$m_{20} = \sum_{l=1}^{Nsm} \left(A^*_{l(i,k)m} - C_{fm} \right) \left(x_{l(i,k)m} - X_0 \right)^2 \tag{2}$$

$$m_{02} = \sum_{l=1}^{Nsm} \left(A^*_{l(i,k)m} - C_{fm} \right) \left(y_{l(i,k)m} - Y_0 \right)^2 \tag{3}$$

$$m_{11} = \sum_{l=1}^{Nsm} \left(A^*_{l(i,k)m} - C_{fm} \right) \left(y_{l(i,k)m} - Y_0 \right) \left(x_{l(i,k)m} - X_0 \right) \tag{4}$$

X_0, Y_0 are the first-order moments:

$$X_0 = \frac{\sum_{l=1}^{Nsm} \left(A^*_{l(i,k)m} - C_{fm} \right) x_{l(i,k)m}}{A^*_{\Sigma m}} \tag{5}$$

$$Y_0 = \frac{\sum_{l=1}^{Nsm} \left(A^*_{l(i,k)m} - C_{fm} \right) y_{l(i,k)m}}{A^*_{\Sigma m}} \tag{6}$$

$x_{l(I,k)m}$, $y_{l(I,k)m}$ are the coordinates of the $l(i, k)$-th pixel of the m-th single image of the object.

The length L_m of the object image is computed as:

$$L_m = \sqrt{\left(x_{m\max} - x_{m\min} \right)^2 + \left(y_{m\max} - y_{m\min} \right)^2} \tag{7}$$

where $x_{m\max}$, $y_{m\max}$, $x_{m\min}$, and $y_{m\min}$ are the minimum and maximum values of the abscissa and ordinates of the m-th intraframe processing area.

The inclination angle ω_j of the j-th object is computed as:

$$\omega_j = \frac{1}{2} \arctan \frac{2m_{11}}{m_{20} - m_{02}} \tag{8}$$

Using Eqs. (1), (7), and (8), we can compute the typical shape of each object image in the CCD frame.

E. Classification of Object Images

The classification of segmented contours in object images into different pattern types forms the foundation for astronomical knowledge discovery in databases as well as data mining [33].

It can be used for photometric integrity checks, with further applications in object recognition [34], motion detection [35], and analysis.

Classifying object image shapes in CCD frames involves grouping the appearances of Solar System objects according to their physical and optical properties, observational conditions, and instrumental influences.

This process supports a better understanding of the objects' nature and helps optimize imaging techniques for their investigation.

The classification of object images in astronomical CCD frames is not only an auxiliary step but also a critical prerequisite for automating subsequent computational tasks.

Accurate separation of circular, elongated, intersecting, and blurred images (Fig. 5) into distinct categories allows algorithms to apply tailored methods of processing and analysis.

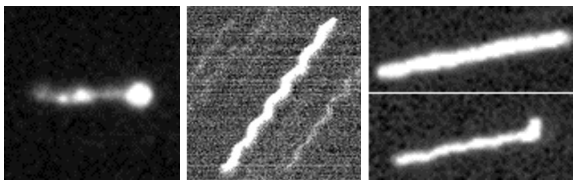

Fig. 5. Examples of blurred images.

For instance, characterizing elongated streaks as fast-moving satellites or debris objects enables the development of specialized detection pipelines [36].

At the same time, the identification of circular point-like patterns facilitates precise photometry of variable stars [37] and asteroids.

Without a robust classification stage, errors may propagate through the processing chain, degrading both positional accuracy and the reliability of physical interpretations.

Furthermore, classification enhances the efficiency of large-scale surveys by reducing ambiguity in data interpretation. With the increasing volume of astronomical imagery generated by modern sky surveys and space monitoring systems, manual inspection becomes infeasible.

Automated classification ensures scalability, enabling real-time filtering of frames and prioritization of potentially rare or hazardous objects, such as near-Earth asteroids or untracked space debris [38]. This capability is significant for early-warning systems, where rapid decisions must be made based on the type of segmented image.

Equally important, classification supports the evaluation of observational biases. By distinguishing between blurred or intersected images and well-resolved circular sources, researchers can identify frames affected by atmospheric turbulence, tracking errors, or optical distortions [39].

This, in turn, helps refine calibration procedures, correct for systematic uncertainties, and assess the overall quality of the observational campaign. Thus, classification not only organizes observational data but also safeguards the scientific validity of subsequent measurements [40].

IV. Result and Discussion

A. Observational Instrumentation

During the study, several hundred analytical models were developed to represent various object image shapes observed in astronomical frames. These frames were acquired using data from multiple telescopes that have official Minor Planet Center (MPC) code: AZT8 (MPC code B17) (Fig. 6a), Sazhen-S (MPC code L18) (Fig. 6b), OMT-800 (MPC code 583) (Fig. 7a), and Takahashi BRC-250M (MPC code K99) (Fig. 7b).

(a) (b)

Fig. 6. Telescopes under research: a) AZT8 (MPC code B17); b) Sazhen-S (MPC code L18).

a) b)

Fig. 7. Telescopes under research: a) OMT-800 (MPC code 583); b) Takahashi BRC-250M (MPC code K99).

B. Astronomical Examples

Some real examples of the proposed astronomical image segmentation process for nearby circular objects in computer vision, which facilitates automated object detection and classification, are presented in Fig. 8.

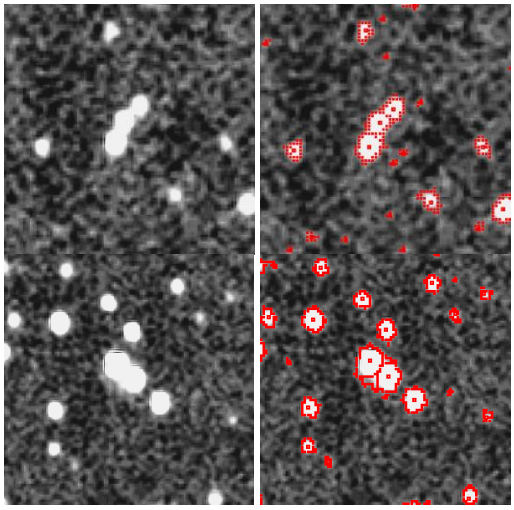

Fig. 8. Segmentation of the nearby circular objects' images.

Fig. 9 shows examples of different types of objects' images in a CCD frame, along with their 3D demonstrations: intersection with near objects, objects with blurred borders, objects with diffraction rays, and fast-moving objects.

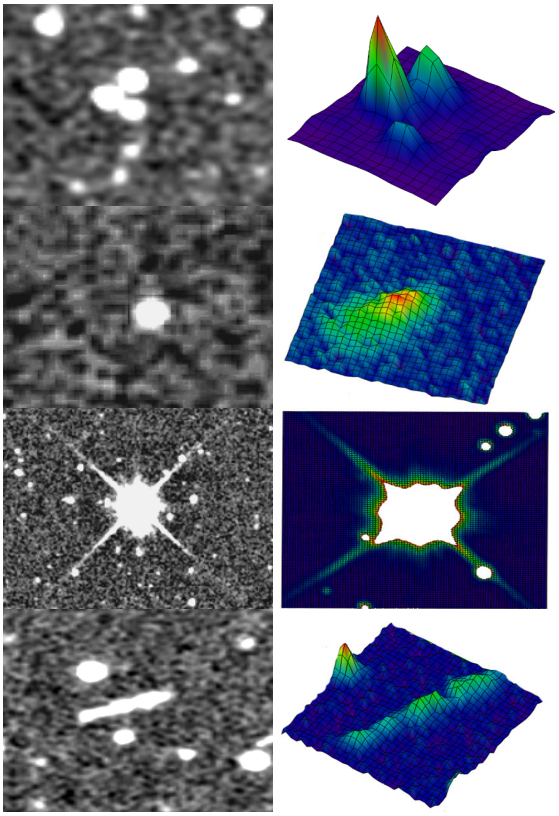

Fig. 9. Different types of objects' images in a CCD frame.

During the research, a lot of series of frames were analyzed. Below in Figs. 10–13 are some examples of the image fragments from different telescopes with the formed analytical models and generated typical shapes.

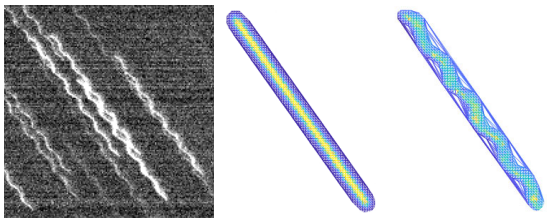

a) b) c)

Fig. 10. Sazhen-S telescope: a) original image; b) analytical model; c) generated typical shape model.

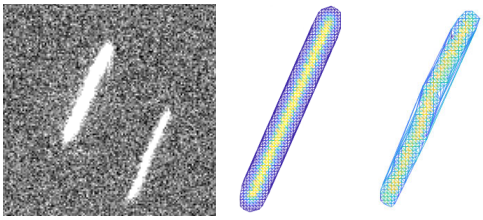

a) b) c)

Fig. 11. OMT-800 telescope: a) original image; b) analytical model; c) generated typical shape model.

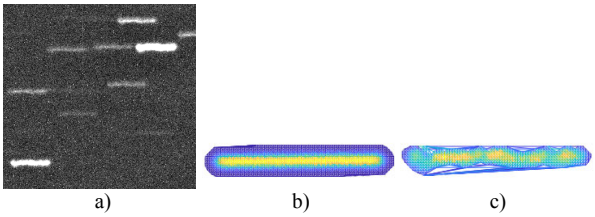

a) b) c)

Fig. 12. AZT8 telescope: a) original image; b) analytical model; c) generated typical shape model.

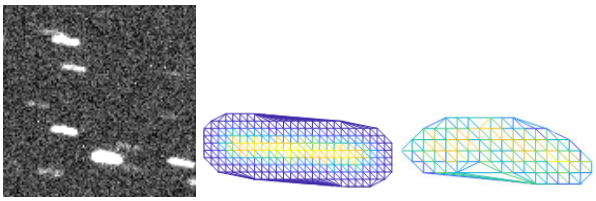

a) b) c)

Fig. 13. Takahashi BRC-250M telescope: a) original image; b) analytical model; c) generated typical shape model.

C. Statistical Evaluation

The primary statistical criterion for evaluating accuracy in this research was the Root Mean Square (RMS) of brightness.

This metric represents the difference between the experimentally observed brightness values, obtained from various major astronomical catalogs [41], and the corresponding pixel brightness values in the analytical model of the object's image:

$$\sigma_{\Delta Aj} = \sqrt{\frac{1}{N_j}\sum_{i=1}^{N_j}\left(A_i^* - A_i\right)^2} \qquad (9)$$

where A_i^* and A_i are the experimental and model brightness of the i-th pixel of the object image;

N_j is the number of pixels in the image of the j-th object in the frame.

Tables I and II present the RMS characteristics, denoted as $\sigma_{\Delta Aj}$, which quantify the difference between the experimental and modeled pixel brightness values for all blurred object images in the frame.

Table I presents the accuracy indicators for object images whose typical shapes can be analytically described using common recognition patterns, such as circular or elliptical forms.

TABLE I. ANALYTICALLY DEFINED TYPICAL SHAPE

Telescope	N of objects	$M\sigma_{\Delta A}$, ADU	$M_{½}\sigma_{\Delta}A$, ADU	$max\sigma_{\Delta A}$, ADU	$min\sigma_{\Delta A}$, ADU
Sazhen-S	173	182.37	37.24	1061.73	2.25
OMT-800	78	7.91	4.52	31.42	0.71
AZT8	157	67.35	5.71	1587.78	0.43
Takahashi BRC-250M	536	14.51	3.82	1061.24	1.27

In contrast, Table II provides corresponding indicators for object images whose shapes were computed based on individual parameters, specifically the object's eccentricity, image length, and inclination angle.

TABLE II. COMPUTED TYPICAL SHAPE

Telescope	N of objects	$M\sigma_{\Delta A}$, ADU	$M_{½}\sigma_{\Delta}A$, ADU	$max\sigma_{\Delta A}$, ADU	$min\sigma_{\Delta A}$, ADU
Sazhen-S	173	61.54	12.52	548.58	2.17
OMT-800	78	4.38	2.35	19.17	0.34
AZT8	157	22.34	3.18	1342.18	0.22
Takahashi BRC-250M	536	11.95	3.21	238.75	0.31

This distinction allows for a comparative evaluation of segmentation accuracy between analytically predefined and parametrically derived object shapes.

Specifically, the tables include the following metrics: the average RMS value $\sigma_{\Delta A}$ of the brightness difference across the frame, $M\sigma_{\Delta A}$; the median RMS value, $M_{1/2}\sigma_{\Delta}A$; the maximum value of RMS differences, $max\sigma_{\Delta A}$; and the minimum value, $min\sigma_{\Delta A}$.

These indicators provide a comprehensive statistical overview of the model's accuracy in representing the observed pixel brightness (Fig. 14).

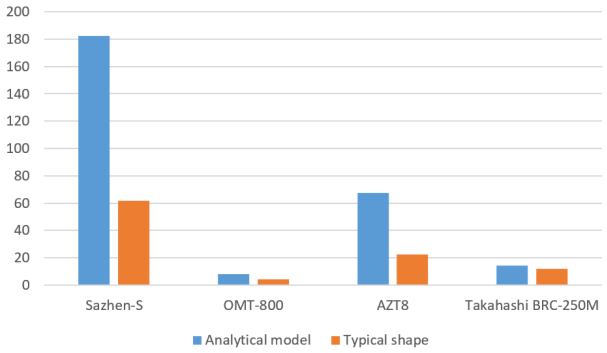

Fig. 14. Accuracy indicators (RMS) for analytical model and typical shape model.

Analysis of the accuracy indicators (RMS) for analytical model and typical shape model shows that the typical shape model increases the accuracy up to 30%.

For additional evaluation of the classification performance, the following quantitative indicators were also used: classification accuracy and recall rate. These quantitative indicators were calculated based on the confusion matrix.

Classification accuracy represents the proportion of correctly identified images among all classified samples. It was calculated as the ratio of the sum of True Positive (TP) and True Negative (TN) decisions to the total number of analyzed cases, which also included False Positive (FP) and False Negative (FN) classifications.

This metric provided a general measure of how well the classifier performs across all recognition patterns (analytical model) and typical shape models.

During research we received the following classification accuracy: 74% for analytical models and 96% for typical shape models.

Recall rate, also known as sensitivity, indicated the ability of the classifier to correctly identify all instances belonging to a particular class and recognition pattern. It was defined as the ratio of TP to the sum of TP and FN.

Table III shows the recall rate for analytical and typical shape models for the different types of classes/patterns.

TABLE III. RECALL RATE

Model	Circular	Elongated	Intersection	Blurred
Analytical	0.93	0.84	0.62	0.58
Typical shape	0.99	0.97	0.95	0.91

A high recall value demonstrates that most of the relevant objects were successfully detected, which is especially important in applications such as object or anomaly detection where missing a target may be critical.

V. CONCLUSION

The increasing volume of data from modern astronomical surveys necessitates reliable and efficient methods for automated object segmentation, detection and classification in CCD frames. This study has presented an integrated approach to astronomical image segmentation that combines classical image processing techniques with modern computer vision strategies.

The developed method effectively addresses common challenges, such as background noise, low contrast, and overlapping sources, enabling the reliable detection of both point-like and extended objects during the data mining process and knowledge discovery in databases.

Through adaptive thresholding, background subtraction, and morphological operations, the segmentation and classification pipeline isolates candidate objects and extracts their contours, facilitating the recognition of key image patterns.

These patterns—ranging from circular and elongated to intersecting and blurred—enable precise object classification using shape, intensity, and spatial features. The segmentation framework supports downstream tasks including astrometry, photometry, object identification, and motion tracking.

The proposed approach has been implemented in the Lemur software, developed as part of the CoLiTec project (Collection Light Technology) (https://colitec.space). Lemur has been successfully deployed in long-term observation programs at several observatories worldwide.

The Lemur software processes CCD data streams in fully automated mode, performing pre-processing, segmentation, post-segmentation and classification analysis in real-time.

During the research, observational data were collected from several telescopes, including AZT-8 (MPC code B17), Sazhen-S (MPC code L18), OMT-800, and Takahashi BRC-250M (MPC code K99).

These instruments provided astronomical CCD frames with varied optical characteristics and seeing conditions, enabling comprehensive testing and validation of the proposed segmentation, classification, and analytical modeling techniques, as well as the proposed method for computing typical shapes across diverse observational setups.

As a result of this implementation, the RMS error of astrometric measurements has decreased by a factor of two, significantly improving the accuracy of object localization and orbit determination.

In operational use, Lemur has contributed to the discovery of more than 1700 asteroids, including five NEOs, 21 Jupiter Trojan asteroids, and one Centaur, as well as the detection of five new comets.

In total, the developed Lemur software has been used in over 800,000 observations, demonstrating its robustness and scalability for wide-field automated sky surveys.

The trial versions of the latest Lemur software for both Windows and Linux, along with comprehensive user guides and documentation, are freely available for download at https://colitec.space/en-download.

Additionally, demo series test data (including raw and processed frames) and configuration files required for processing can be freely accessed at https://colitec.space/en-demo.

Overall, this work emphasizes the importance of segmentation as a foundational step in astronomical image analysis, bridging raw observational data with high-level scientific insights through automated and scalable processing techniques.

CONFLICT OF INTEREST

The authors declare no conflict of interest.

AUTHOR CONTRIBUTIONS

V.E.S. conducted the conceptualization, methodology and project administration; V.E.S., S.V.K. and V.P.V. developed mathematical algorithms and methods; O.B.B. and V.P.V. developed the modules of software; V.P.V. and T.O.T. performed the validation and formal analysis; S.V.K. and T.O.T. wrote the paper; all authors had approved the final version.

FUNDING

The research was supported by the Ukrainian project of fundamental scientific research, “Development of computational methods for detecting objects with near-zero and locally constant motion by optical-electronic devices” (#0124U000259) from 2024 to 2026.

ACKNOWLEDGMENT

The authors express their sincere gratitude to the dedicated observers and astronomical teams whose telescopes and observational efforts made this research possible by providing high-quality CCD image data and supporting long-term monitoring campaigns.

We acknowledge the continuous collaboration and technical contributions from all astronomers who participated in data acquisition, telescope operation, and observation planning.

REFERENCES

[1] V. Savanevych *et al.*, "Mathematical methods for an accurate navigation of the robotic telescopes," *Mathematics*, vol. 11, no. 10, 2246, 2023. doi: 10.3390/math11102246

[2] D. Oszkiewicz *et al.*, "Spins and shapes of basaltic asteroids and the missing mantle problem," *Icarus*, vol. 357, 114158, 2021. doi: 10.1016/j.icarus.2020.114158

[3] S. Khlamov *et al.*, "The astronomical object recognition and its near-zero motion detection in series of images by in situ modeling," in *Proc. the International Conference on Systems, Signals, and Image Processing*, 2022. doi: 10.1109/IWSSIP55020.2022.9854475

[4] V. Troianskyi *et al.*, "First reported observation of asteroids 2017 AB8, 2017 QX33, and 2017 RV12," *Contr. of the Astron. Obs. Skalnate Pleso*, vol. 53, no. 2, pp. 5–15, 2023. doi: 10.31577/caosp.2023.53.2.5

[5] D. Oszkiewicz *et al.*, "Spin rates of V-type asteroids," *A&A*, vol. 643, A117, 2020. doi: 10.1051/0004-6361/202038062

[6] J-L. Starck and F. Murtagh, *Astronomical Image and Data Analysis*, 2nd ed. Astronomy and Astrophysics Library, Springer, 2007.

[7] R. Gonzalez and R. Woods, *Digital Image Processing*, 4th ed. NY: Pearson, 2018.

[8] C. Steger *et al.*, *Machine Vision Algorithms and Applications*, John Wiley & Sons, 2018.

[9] G. Adam *et al.*, "Embedded microcontroller with a CCD camera as a digital lighting control system," *Electronics*, vol. 8, no. 1, p. 33, 2019. doi: 10.3390/electronics8010033

[10] M. Bellanger, *Digital Signal Processing: Theory and Practice*, Wiley, 2024, p. 400.

[11] L. Mykhailova *et al.*, "Method of maximum likelihood estimation of compact group objects location on CCD-frame," *EEJET*, vol. 5, no. 4, pp. 16–22, 2014. doi: 10.15587/1729-4061.2014.28028

[12] Š. Parimucha *et al.*, "CoLiTecVS—A new tool for an automated reduction of photometric observations," *Contr. of the Astron. Obs. Skalnate Pleso*, vol. 49, no. 2, pp. 151–153, 2019.

[13] V. Akhmetov *et al.*, "Cloud computing analysis of Indian ASAT test on March 27, 2019," in *Proc. the IEEE International Scientific-Practical Conference: PIC S&T*, 2019, pp. 315–318. doi: 10.1109/PICST57299.2022.10238587

[14] E. Dougherty, *Digital Image Processing Methods*, CRC Press, 2020, p. 504.

[15] Y. Zhang *et al.*, "Data mining and knowledge discovery in database of astronomy," *Progress in Astronomy*, vol. 20, no. 4, pp. 312–323, 2002.

[16] S. Khlamov *et al.*, "Astronomical image processing by the Lemur software," in *Proc. the 6th Asia Conference on Machine Learning and Computing, ACMLC*, 2025, pp. 139–145. doi: 10.1145/3690771.3690801

[17] S. Khlamov *et al.*, "Machine vision for astronomical images using the modern image processing algorithms implemented in the CoLiTec software," *Measurements and Instrumentation for Machine Vision*, Chapter 12: CRC Press, pp. 269–310, 2024. doi: 10.1201/9781003343783-12

[18] V. Akhmetov *et al.*, "Astrometric reduction of the wide-field images," *Advances in Intelligent Systems and Computing*, vol. 1080, pp. 896–909, 2020. doi: 10.1007/978-3-030-33695-0_58

[19] V. Savanevych *et al.*, "CoLiTecVS software for the automated reduction of photometric observations in CCD-frames," *Astronomy and Computing*, vol. 40, 100605, 2022. doi: 10.1016/j.ascom.2022.100605

[20] R. F. Haack *et al.*, "The S-PLUS Fornax Project (S+FP): SExtractor detection and measurement of nearby galaxies in large photometric surveys," *MNRAS*, vol. 530, no. 3, pp. 3195–3207, 2024. doi: 10.1093/mnras/stae1053

[21] G. Bifeng *et al.*, "Applications and technology research for Astrometrica and MaxIm DL in astrometry," *Astronomical Techniques and Instruments*, vol. 18, no. 2, pp. 195–202, 2021. doi: 10.14005/j.cnki.issn1672-7673.20200701.001

[22] J. Ascencio-Moran *et al.*, "Experience in asteroid search using Astrometrica software," *International Journal of Advanced Computer Science and Applications*, vol. 10, no. 5, pp. 455–460, 2019. doi: 10.14569/IJACSA.2019.0100558

[23] S. Khlamov *et al.*, "Development of the matched filtration of a blurred digital image using its typical form," *Eastern-European Journal of Enterprise Technologies*, vol. 1, no. 9–121, pp. 62–71, 2023. doi: 10.15587/1729-4061.2023.273674

[24] Y. M. Al-Sharo *et al.*, "Neural networks as a tool for pattern recognition of fasteners," *International Journal of Engineering Trends and Technology*, vol. 69, no. 10, pp. 151–160, 2021. doi: 10.14445/22315381/IJETT-V69I10P219

[25] S. Minaee *et al.*, "Image Segmentation using deep learning: A survey," *IEEE Transactions on Pattern Analysis and Machine Intelligence*, vol. 44, no. 7, pp. 3523–3542, 2021. doi: 10.1109/TPAMI.2021.3059968

[26] L. Kirichenko *et al.*, "Classification of time realizations using machine learning recognition of recurrence plots," *Adv. in Intel. Syst. and Comp.*, vol. 1246, pp. 687–696, 2021. doi: 10.1007/978-3-030-54215-3_44

[27] Y. Bodyanskiy *et al.*, "Adaptive least-squares support vector machine and its combined learning-selflearning in image recognition task," in *Proc. the 17th International Scientific and Technical Conference on CSIT*, 2022, pp. 48–51. doi: 10.1109/CSIT56902.2022.10000518

[28] S. Khlamov *et al.*, "Big data analysis in astronomy by the Lemur software," in *Proc. the IEEE 6th International Conference on Inform. and Telecom. Technol. and Radio Electronics*, 2023, pp. 5–8. doi: 10.1109/UkrMiCo61577.2023.10380398

[29] V. Kudak *et al.*, "Determining the orientation and spin period of TOPEX/Poseidon satellite by a photometric method," *Astr. Bul.*, vol. 72, no. 3, pp. 340–348, 2017. doi: 10.1134/S1990341317030233

[30] V. Akhmetov *et al.*, "Fast coordinate cross-match tool for large astronomical catalogue," *Adv. in Intel. Syst. and Comp.*, vol. 871, pp. 3–16, 2019. doi: 10.1007/978-3-030-01069-0_1

[31] S. Khlamov *et al.*, "Automated data mining of the reference stars from astronomical CCD frames," *CEUR Workshop Proceedings*, vol. 3668, pp. 83–97, 2024. doi: 10.31110/colins/2024-2/007

[32] V. Troianskyi *et al.*, "Optical observations of the potentially hazardous asteroid (4660) Nereus at opposition 2021," *Icarus*, vol. 420, 116146, 2024. doi: 10.1016/j.icarus.2024.116146

[33] Q. Luo, "Advancing knowledge discovery and data mining," in *Proc. the International Workshop on Knowledge Discovery and Data Mining*, 2008, pp. 3–5. doi: 10.1109/WKDD.2008.153

[34] S. Khlamov *et al.*, "Recognition of the astronomical images using the Sobel filter," in *Proc. the International Conference on Systems, Signals, and Image Processing*, 2022. doi: 10.1109/IWSSIP55020.2022.9854425

[35] V. Savanevych *et al.*, "A method of immediate detection of objects with a near-zero apparent motion in series of CCD-frames," *A&A*, vol. 609, A54, 2018. doi: 10.1051/0004-6361/201630323

[36] E. Hadzhyiev *et al.*, "Application of docker compose for constructing the infocommunication system for online processing of astronomical images," in *Proc. the International Conference on Advanced Computer Information Technologies*, 2025. doi: 10.1109/ACIT65614.2025.11185586

[37] I. Kudzej *et al.*, "CoLiTecVS—A new tool for the automated reduction of photometric observations," *Astronomische Nachrichten*, vol. 340, no. 1–3, pp. 68–70, 2019. doi: 10.1002/asna.201913562

[38] D. Oszkiewicz *et al.*, "Spins and shapes of basaltic asteroids and the missing mantle problem," *Icarus*, vol. 397, 115520, 2023. doi: 10.1016/j.icarus.2023.115520

[39] V. Vlasenko *et al.*, "Devising a procedure for the brightness alignment of astronomical frames background by a high frequency filtration to improve accuracy of the brightness estimation of objects," *EEJET*, vol. 2, no. 2–128, pp. 31–38, 2024. doi: 10.15587/1729-4061.2024.301327

[40] H. Yang *et al.*, "Data mining techniques on astronomical spectra data-II. Classification analysis," *MNRAS*, vol. 518, no. 4, pp. 5904–5928, 2022. doi: 10.1093/mnras/stac3292

[41] I. Vavilova *et al.*, *Surveys, Catalogues, Databases, and Archives of Astronomical Data*, *Knowledge Discovery in Big Data from Astronomy and Earth Observation*, Elsevier, 2020, pp. 57–102, 2020. doi: 10.1016/B978-0-12-819154-5.00015-1